Robust Hybrid Beamforming for Full-Duplex OFDM mmWave Systems with Partially-Connected Structure

Zhen Luo[1,2], Yanzi Hu[1(✉)], Yangfan Xiang[1], and Hongqing Liu[1]

[1] The School of Communication and Information Engineering, Chongqing University of Posts and Telecommunications, Chongqing 400065, China
yanzihu09@163.com

[2] College of Electronic and Information Engineering, Southwest University, Chongqing 400715, China

Abstract. In this paper, a full-duplex orthogonal frequency division multiplexing (OFDM) millimeter wave systems with correlated estimation errors and partially-connected structures is investigated to improve the spectral efficiency and energy efficiency. To attenuate the self-interference caused by full-duplex mode, a zero-space projection based method is proposed. Then, a two-stage hybrid beamforming scheme is developed. In the fist stage, the correlated channel estimation errors are considered to design the robust fully digital beamformers. In the second stage, an alternating algorithm with closed-form solutions is proposed to solve the hybrid processors. The numerical results show that the proposed scheme has superior performance over existing designs.

Keywords: mmWave · hybrid beamforming · full-duplex · partially-connected · OFDM · correlated estimation errors

1 Introduction

The combination of characteristics of millimeter wave (mmWave) signals and massive multiple-input multiple-output (MIMO) architectures can obtain considerable system gains to combat the severe path loss. For conventional massive MIMO systems with fully digital beamformers, each transmitting or receiving antenna need to assign one radio frequency (RF) chain. Applying such structure to mmWave systems with large antenna arrays results in extremely high power consumption and hardware complexity. Thus, the hybrid analog and digital beamforming structure has been commonly adopted in mmWave systems due to its high system gains and low hardware complexity compared to fully digital beamforming techniques [1].

The full-duplex (FD) communication mode based mmWave systems has the potential to further improve the spectral efficiency by supporting simultaneous transmission and reception. It can nearly achieve twice the spectral efficiency

F. Gao et al. (Eds.): ChinaCom 2022, LNICST 500, pp. 191–203, 2023.
https://doi.org/10.1007/978-3-031-34790-0_15

of the half-duplex (HD) mode. Whereas, the severe self-interference (SI) caused by the co-frequency co-time transmission makes the spectral efficiency far less than expected [2]. SI cancellation (SIC) based on the hybrid beamforming has been studied in the literature. In [3,4], passive SIC schemes at the base station are adopted by utilize RF absorber material and cross-polarization. Hence, the SI channel is considered as a far-field transmission channel. The FD scheme at the base station is proposed for the cellular system in [3], by scheduling the uplink and downlink single-antenna HD users based on the beam-domain distributions of the associated channels to mitigate the SI. The beam-domain based SIC scheme is extended in [4] to design a hybrid time switching and power splitting simultaneous wireless information and power transfer protocol for the FD base station.

However, the line-of-sight (LoS) SI channel cannot be ignored in mmWave systems due to the antenna placement and device packaging [5]. Considering the LoS SI channel, a zero-space projection based SIC method is proposed in [6] to eliminate the SI by replacing the digital beamformer with the vectors in the zero-space of the analog equivalent channel. In [7], the widespread hybrid beamforming design procedure is adopted in point-to-point FD mmWave systems. The fully digital processors and the hybrid processors are solved sequentially. This design procedure would result in a sub-optimal solution, but it is attractive for its ease of use. It has been utilized to design hybrid beamforming schemes for multi-user FD orthogonal frequency division multiplexing (OFDM) mmWave systems in [8]. The aforementioned works all adopt fully-connected structures in which each RF chain is connected to all antennas. However, such a structure leads to severe insertion losses and degrades the energy efficiency [9]. Thus, the partially-connected structure, in which each RF chain is only connected with part of the antennas with fewer phase shifters, is more attractive in energy efficiency sensitive scenarios. In [10], an alternating minimization algorithm is proposed to decompose the fully digital processors into hybrid ones with partially-connected structures.

It is noted that the above designs are restricted to perfect channel state information (CSI) assumptions, which is impractical due to the imperfect channel estimations. The robust hybrid FD beamforming designs dealing with imperfect channel estimates are reported in [11]. However, the users therein are all equipped with single-antenna, and the estimation errors are assumed to be independent and identically distributed (i.i.d.). The general Kronecker model of the estimated channel is adopted in [12], and the robust beamformers are investigated for mmWave HD relay systems. To our best knowledge, energy efficient hybrid beamforming designs for FD broadband mmWave systems that are robust to correlated channel estimation errors have not been investigated yet.

In this paper, we develop a robust hybrid beamforming designs with partially-connected structure for point-to-point FD OFDM mmWave systems. First, a zero-space projection based method is proposed to mitigate the SI, and the fully digital robust beamformers are optimized based on the general estimated channel model. According to the relationship between the lower bound of averaged

mutual information and the weighted minimum mean squared error (WMMSE), the original highly complicated optimization problem is transformed into a tractable one. To improve the energy efficiency, an alternating method is utilized to decompose the fully digital processors into hybrid ones with partially-connected structures. The performances of the proposed hybrid beamformers and SIC scheme are examined by numerical simulations.

2 System and Channel Model

2.1 System Model

Consider a point-to-point FD OFDM mmWave system, where one node with N_i, $i \in \{a, b\}$ antennas and $N_{i,rf}$ RF chains transmit $N_{i,s}$ data streams to another node that has M_i antennas and $M_{i,rf}$ RF chains. The above parameters are subject to constraints $N_{i,s} \leq N_{i,rf} \leq N_i$, $N_{i,s} \leq M_{i,rf} \leq M_i$. Node a and node b are all operating in FD mode, and both of them adopt hybrid analog-digital beamformers with partially-connected structure. We assume the data stream numbers of node a and node b are identical.

At the transmitter, the transmitted signal vector $\mathbf{s}_i[k] \in \mathbb{C}^{N_{i,s}\times 1}$ of node i at k^{th} subcarrier $k = 1, ..., K$, is first fed into the digital precoder, $\mathbf{F}_{i,bb}[k] \in \mathbb{C}^{N_{i,rf}\times N_{i,s}}$. Then the precoded signals are transformed into time-domain using inverse fast Fourier transformations (IFFTs). After adding proper cyclic prefix (CP), the processed signals are phase-shifted using the following analog beamformer matrix $\mathbf{F}_{i,t} \in \mathbb{C}^{N_i\times N_{i,rf}}$. At the receiver side, assuming perfect carrier and frequency offset synchronization, the received signals for each subcarrier are processed using the analog combiner $\mathbf{W}_{i,r} \in \mathbb{C}^{M_i\times M_{i,rf}}$. Then, the CP is removed and the signals in time-domain are transformed into frequency-domain through the fast Fourier transformation (FFT). Finally, the combiner $\mathbf{W}_{i,bb}[k] \in \mathbb{C}^{M_{i,rf}\times N_{i,s}}$ is employed to obtain the processed signal at the k^{th} subcarrier. The received signal vector of node i at k^{th} sub-carrier is given by

$$\begin{aligned}\mathbf{y}_i[k] = &\underbrace{\sqrt{P_j}\mathbf{W}_{i,bb}^H[k]\mathbf{W}_{i,r}^H\mathbf{H}_{ji}[k]\mathbf{F}_{j,t}\mathbf{F}_{j,bb}[k]\mathbf{s}_j[k]}_{\text{desired signal}} \\ &+ \underbrace{\sqrt{P_{i,si}}\mathbf{W}_{i,bb}^H[k]\mathbf{W}_{i,r}^H\mathbf{H}_{i,si}[k]\mathbf{F}_{i,t}\mathbf{F}_{i,bb}[k]\mathbf{s}_i[k]}_{\text{SI}} \\ &+ \underbrace{\mathbf{W}_{i,bb}^H[k]\mathbf{W}_{i,r}^H\mathbf{n}_i[k]}_{\text{noise}},\end{aligned} \tag{1}$$

where $i, j \in \{a, b\}, i \neq j$; P_j and $P_{i,si}$ denote the transmit power of node j and the SI power of node i, respectively. The transmitted signal vector $\mathbf{s}_j[k]$ is subject to $E\left\{\mathbf{s}_j[k]\mathbf{s}_j^H[k]\right\} = \mathbf{I}_{N_{j,s}}$. $\mathbf{H}_{ji}[k] \in \mathbb{C}^{M_i\times N_j}$ is the mmWave channel matrix from the transmitter of node j to the receiver of node i at the k^{th} subcarrier; $\mathbf{H}_{i,si}[k] \in \mathbb{C}^{M_i\times N_i}$ is the SI channel matrix of node i at the k^{th} sub-carrier; $\mathbf{n}_i[k]$ is the additive complex white Gaussian noise (AWGN) vector of node i at the k^{th} subcarrier with zero mean and covariance matrix $\delta_i^2\mathbf{I}$.

It is worth noting that the analog processor is a post-IFFT module, so it is identical for all subcarriers, which is the key challenge of hybrid beamformer designs in broadband mmWave systems. Furthermore, every element in the analog processing matrices has an equal modulus, i.e., $|\mathbf{F}_{i,t}^{(m,n)}|^2 = |\mathbf{W}_{i,r}^{(m,n)}|^2 = 1, \forall m, n$.

2.2 Channel Model

The geometric channel model that incorporating the wideband and limited scattering characteristics of mmWave channel is adopted in this paper. The delay-d channel matrix from the transmitter of node j to the receiver of node i with uniform linear arrays (ULAs) is given by [13]

$$\mathbf{H}_{ji}[d] = \sqrt{\frac{N_j M_i}{N_p}} \sum_{l=1}^{N_p} \alpha_{ji,l} p\left(dT_s - \tau_l\right) \mathbf{a}_r\left(\theta_{ji,l}^r\right) \mathbf{a}_t^H\left(\theta_{ji,l}^t\right) \tag{2}$$

where N_j and M_i are the numbers of transmit and receive antenna arrays, N_p is the number of propagation paths. $p(\tau)$ denotes the pulse shaping filter with T_s-spaced signalling evaluated at τ seconds. $\alpha_{ji,l} \sim \mathcal{CN}(0,1)$ denotes the complex gain of the l^{th} path. $\mathbf{a}_r\left(\theta_{ji,l}^r\right)$ and $\mathbf{a}_t\left(\theta_{ji,l}^t\right)$ are the normalized receive and transmit array response vectors with the azimuth angle of arrival (AoA) and departure (AoD) $\theta_{ji,l}^r$ and $\theta_{ji,l}^t$, respectively. The vector $\mathbf{a}_r\left(\theta_{ji,l}^r\right)$ and $\mathbf{a}_t\left(\theta_{ji,l}^t\right)$ can be expressed as

$$\mathbf{a}_r\left(\theta_{ji,l}^r\right) = \frac{1}{\sqrt{N_r}} \left[1 \quad e^{j\pi \sin\theta_{ji,l}^r} \quad \ldots \quad e^{j\pi(N_r-1)\sin\theta_{ji,l}^r}\right]^T \tag{3}$$

$$\mathbf{a}_t\left(\theta_{ji,l}^t\right) = \frac{1}{\sqrt{N_t}} \left[1 \quad e^{j\pi \sin\theta_{ji,l}^t} \quad \ldots \quad e^{j\pi(N_t-1)\sin\theta_{ji,l}^t}\right]^T \tag{4}$$

Assuming perfect synchronization, the channel matrix at k^{th} sub-carrier can be expressed as [13]

$$\begin{aligned} \mathbf{H}_{ji}[k] &= \sum_{d=0}^{D-1} \mathbf{H}_{ji}[d] e^{-\frac{j2\pi kd}{K}} \\ &= \sqrt{\frac{N_j M_i}{N_p}} \sum_{l=1}^{N_p} \alpha_{ji,l} \mathbf{a}_r\left(\theta_{ji,l}^r\right) \mathbf{a}_t^H\left(\theta_{ji,l}^t\right) \times \sum_{d=0}^{D-1} p\left(dT_s - \tau_l\right) e^{-\frac{j2\pi kd}{K}} \end{aligned} \tag{5}$$

Considering the antenna placement and size of mmWave devices, the SI channel matrix of node i at the k^{th} subcarrier $\mathbf{H}_{i,si}[k]$ is given by [5]

$$\mathbf{H}_{i,si}[k] = \sqrt{\frac{\kappa}{1+\kappa}} \mathbf{H}_{i,los} + \sqrt{\frac{1}{1+\kappa}} \mathbf{H}_{ii}[k], \tag{6}$$

where κ is the Rician factor; $\mathbf{H}_{ii}[k]$ is the reflected path component of the SI channel at k^{th} subcarrier, which can be modelled as Eq. (5) with corresponding

AoAs and AoDs; The LoS component of the SI channel, $\mathbf{H}_{i,los}$, is adopted to a frequency flat near-field model. For more details please refer to [5].

Due to the packaging of a FD mmWave device, the propagation circumstances of the LoS component are basically stable [5]. So we assume an accurate estimation of $\mathbf{H}_{i,los}$ in this paper. For other channels, i.e., $\mathbf{H}_{ji}[k]$ and $\mathbf{H}_{ii}[k]$, the general Kronecker model in [12] is adopted, and the estimated channel is given by

$$\mathbf{H}[k]\& = \bar{\mathbf{H}}[k] + \mathbf{T}\boldsymbol{\Delta}\mathbf{R}, \tag{7}$$

where $\mathbf{T}$ and $\mathbf{R}$ are the transmitting and receiving covariance matrices of the channel estimation errors; $\boldsymbol{\Delta} \sim \mathcal{CN}\left(\mathbf{0}, \sigma^2\mathbf{I}\right)$ is the unknown part of the channel mismatch, with σ^2 being the variance of estimation errors. Here we drop the subscripts for the ease of notation.

3 Robust Hybrid Beamforming Design

In this section, we first proposed a zero-space projection based SIC method. Under imperfect CSI, the singular value decomposition (SVD) of estimated channel matrix can no longer provide the optimal fully digital beamformers [14]. Then, we derived the optimal fully-digital precoder and combiner by utilizing the relationship between the lower bound of mutual information and the WMMSE. After obtaining the fully-digital beamformers, we decompose them into hybrid ones with partially-connected structures by an alternating decomposition method.

3.1 Self-interference Cancellation

Considering the SI term in Eq. (1), the SIC method should eliminate this term, i.e., $\mathbf{W}_{i,bb}^H[k]\mathbf{W}_{i,r}^H\mathbf{H}_{i,si}[k]\,\mathbf{F}_{i,t}\mathbf{F}_{i,bb}[k] = \mathbf{0}$. Given that the strength of the reflected path component is much weaker than that of the LoS component and the accurate assumption of $\mathbf{H}_{i,los}[k]$, we propose a zero-space projection based SIC method, which is an extension from narrowband systems in [15] to broadband systems. The main difference between these two SIC schemes is the design of analog beamformers, which is common to all sub-carriers. As there is no power constraint at the receiver side, we insert an SIC module, i.e., $\mathbf{W}_{i,sic}$, between the baseband combiner $\mathbf{W}_{i,bb}$ and analog combiner $\mathbf{W}_{i,r}$ to mitigate the interference. The SIC matrix can be designed by finding the zero-space of the equivalent channel.

As we only know the estimated SI channel $\bar{\mathbf{H}}_{i,si}[k]$, we construct the equivalent channel of the k^{th} subcarrier as follows

$$\mathbf{H}_{i,eq}[k] = \mathbf{W}_{i,r}^H\bar{\mathbf{H}}_{i,si}[k]\mathbf{F}_{i,t}\mathbf{F}_{i,bb}[k], \tag{8}$$

By taking the SVD of the above equivalent channel, we have

$$\mathbf{H}_{i,eq}[k] = [\mathbf{U}_{i,eq1}[k] \;\; \mathbf{U}_{i,eq0}[k]]\,\boldsymbol{\Lambda}_{i,eq}[k]\mathbf{V}_{i,eq}^H[k], \tag{9}$$

where $\mathbf{U}_{i,eq1} \in \mathbb{C}^{M_{i,rf} \times N_{i,s}}$ and $\mathbf{U}_{i,eq0} \in \mathbb{C}^{M_{i,rf} \times (M_{i,rf} - N_{i,s})}$ contain the left singular vectors corresponding to non-zero and zero singular values, respectively. $\mathbf{U}_{i,eq0}$ is the zero-space of $\mathbf{H}_{i,eq}$, which satisfies

$$\mathbf{U}_{i,eq0}^{H}[k]\mathbf{H}_{i,eq}[k] = \mathbf{0}, \tag{10}$$

By selecting the corresponding vectors in $\mathbf{U}_{i,eq0}^{H}[k]$, the SIC matrix $\mathbf{W}_{i,sic}$ can be obtained, and the combiner of node i at the k^{th} subcarrier is finally constructed as

$$\mathbf{W}_i[k] = \mathbf{W}_{i,r}\mathbf{W}_{i,sic}[k]\mathbf{W}_{i,bb}[k], \tag{11}$$

The solutions of $\mathbf{W}_{i,r}$ and $\mathbf{W}_{i,bb}[k]$ will be given in Sect. 3.3.

Remark: The necessary condition to preserve the number of data streams after SIC is $\text{rank}(\mathbf{W}_{i,sic}) \geq N_{i,s}$, which is equivalent to $M_{i,rf} \geq 2N_{i,s}$. Otherwise, the number of data streams, i.e., the dimensions of received signal vectors, may be decreased after processing. Compared with the zero-space projection based SIC method in [6], in which the equivalent channel is constructed as $\mathbf{W}_{i,r}^{H}\bar{\mathbf{H}}_{i,si}\mathbf{F}_{i,t}$, the necessary condition to preserve the number of data streams should be $M_{i,rf} \geq N_{i,s} + N_{i,rf}$. Combined with the condition $N_{i,s} \leq \min\{N_{i,rf}, M_{i,rf}\}$, the proposed SIC method requires less RF chains to preserve the number of data streams.

3.2 Fully Digital Beamforming Design

The SI can be effectively attenuated by utilizing the proposed SIC scheme, which will be verified by numerical results in Sect. 4. In this subsection, we design the fully digital beamformers by ignoring the SI term temporarily. Then, the SIC modules is appended to finish the design. By removing the SI term, the combined signal of node i at the k^{th} subcarrier can be written as

$$\mathbf{y}_i[k] = \sqrt{P_j}\mathbf{W}_i^{H}[k]\mathbf{H}_{ji}[k]\mathbf{F}_j[k]\mathbf{s}_j[k] + \mathbf{W}_i^{H}[k]\mathbf{n}_i[k], \tag{12}$$

where $\mathbf{W}_i^{H}[k] = \mathbf{W}_{bb,i}^{H}[k]\mathbf{W}_{i,r}^{H}$ and $\mathbf{F}_j[k] = \mathbf{F}_{j,r}\mathbf{F}_{j,bb}[k]$ represent the fully digital combiner and precoder, respectively.

At the receiver side, the MMSE receiver is adopted, which is given by

$$\begin{aligned}\mathbf{W}_{i,fd}[k] &= \left[E_{\mathbf{H}_{ji}}\left\{\tilde{\mathbf{y}}_i[k]\tilde{\mathbf{y}}_i^{H}[k]\right\}\right]^{-1} E_{\mathbf{H}_{ji}}\left\{\tilde{\mathbf{y}}_i[k]\mathbf{s}_j^{H}[k]\right\} \\ &= \left(P_j\bar{\mathbf{H}}_{ji}[k]\mathbf{F}_j[k]\mathbf{F}_j^{H}[k]\bar{\mathbf{H}}_{ji}^{H}[k] + \mathbf{Q}_i[k]\right)^{-1} \times \sqrt{P_j}\bar{\mathbf{H}}_{ji}[k]\mathbf{F}_j[k]\end{aligned} \tag{13}$$

where $\tilde{\mathbf{y}}_i[k] = \sqrt{P_j}\mathbf{H}_{ji}[k]\mathbf{F}_j[k]\mathbf{s}_j[k] + \mathbf{n}_i[k]$ is the received signal vector before combining of the node i and $\mathbf{Q}_i[k] = P_j\sigma_{ji}^2 \text{tr}\left(\mathbf{T}_j\mathbf{F}_j[k]\mathbf{F}_j[k]^{H}\mathbf{T}_j^{H}\right)\mathbf{R}_i\mathbf{R}_i^{H} + \delta_i^2\mathbf{I}$.

Then, the MMSE matrix can be calculated as

$$\begin{aligned}\mathbf{M}_i[k] &= E_{\bar{\mathbf{H}}_{ji}}\left[\left(\mathbf{W}_{i,fd}^H[k]\tilde{\mathbf{y}}_i[k]-\mathbf{s}_j[k]\right)\left(\mathbf{W}_{i,fd}^H[k]\tilde{\mathbf{y}}_i[k]-\mathbf{s}_j[k]\right)^H\right] \\ &= \mathbf{I}_{N_{i,s}} - P_j\mathbf{F}_j^H[n]\bar{\mathbf{H}}_{ji}^H[n]\left(P_j\bar{\mathbf{H}}_{ji}[k]\mathbf{F}_j^H[k]\bar{\mathbf{H}}_{ji}^H[k]+\mathbf{Q}_i[k]\right)^{-1}\times\bar{\mathbf{H}}_{ji}[k]\mathbf{F}_j[k] \\ &= \left(\mathbf{I}_{N_{i,s}}+P_j\mathbf{F}_j^H[k]\bar{\mathbf{H}}_{ji}^H[k]\mathbf{Q}_i^{-1}[k]\bar{\mathbf{H}}_{ji}[k]\mathbf{F}_j[k]\right)^{-1}\end{aligned} \tag{14}$$

Optimizing the sum rate directly is found to be intractable. In this paper, we adopt the lower bound of mutual information as the objective, which is given by [16]

$$I_{lb}\left(\mathbf{s}_j[k],\tilde{\mathbf{y}}_i[k]\right) = -\log\det\mathbf{M}_i[k], \tag{15}$$

The optimization problem of the fully digital beamformers can be constructed as

$$\begin{aligned}\min_{\{\mathbf{F}_{j,fd}[k]\}} \quad & -\frac{1}{K}\sum_{k=1}^{K}\sum\nolimits_{i,j} I_{lb}\left(\mathbf{s}_j[k],\tilde{\mathbf{y}}_i[k]\right) \\ \text{s.t.} \quad & \mathrm{tr}\left(\mathbf{F}_{j,fd}[k]\mathbf{F}_{j,fd}^H[k]\right)\le 1, i,j\in\{a,b\}, i\neq j\end{aligned} \tag{16}$$

The above problem can be divided into two sub-problems as follows

$$\begin{aligned}\min_{\{\mathbf{F}_{a,fd}[k]\}} \quad & -\frac{1}{K}\sum_{k=1}^{K} I_{lb}\left(\mathbf{s}_a[k],\tilde{\mathbf{y}}_b[k]\right) \\ \text{s.t.} \quad & \mathrm{tr}\left(\mathbf{F}_{a,fd}[k]\mathbf{F}_{a,fd}^H[k]\right)\le 1\end{aligned} \tag{17}$$

$$\begin{aligned}\min_{\{\mathbf{F}_{b,fd}[k]\}} \quad & -\frac{1}{K}\sum_{k=1}^{K} I_{lb}\left(\mathbf{s}_b[k],\tilde{\mathbf{y}}_a[k]\right) \\ \text{s.t.} \quad & \mathrm{tr}\left(\mathbf{F}_{b,fd}[k]\mathbf{F}_{b,fd}^H[k]\right)\le 1\end{aligned} \tag{18}$$

Due to the equivalence of formulas (17) and (18), we just provide the solution for (17) in the next, and the solution for (18) can be obtained by corresponding substitutions. According to [17], the optimization problem (17) is identical to the following WMMSE problem.

$$\begin{aligned}\min_{\{\mathbf{F}_{a,fd}[k],\mathbf{A}_b[k]\}} \quad & \frac{1}{K}\sum_{k=1}^{K}\mathrm{tr}\left(\mathbf{A}_b[k]\mathbf{M}_b[k]\right), \\ \text{s.t.} \quad & \mathrm{tr}\left(\mathbf{F}_{a,fd}[k]\mathbf{F}_{a,fd}^H[k]\right)\le 1.\end{aligned} \tag{19}$$

where $\mathbf{A}_b[k]$ is a weighting matrix. The points are that the KKT conditions of (17) and (19) can be satisfied simultaneously when $\mathbf{A}_b[k]=(\mathbf{M}_b[k])^{-1}$. In the next, we proposed an alternating algorithm to solve (19), and update the fully digital precoder $\mathbf{F}_{a,fd}[k]$, the fully digital combiner $\mathbf{W}_{b,fd}[k]$ and the weighted matrix $\mathbf{A}_b[k]$ iteratively.

Algorithm 1. Proposed design for $\mathbf{F}_{a,fd}[k]$ and $\mathbf{W}_{b,fd}[k]$

Require: Construct $\mathbf{F}_{a,fd}[k]$ randomly; set λ_{min}, λ_{max}, and the termination criteria ϵ_1 and ϵ_2;
repeat
  Calculate $\mathbf{W}_{b,fd}[k]$ according to Eq. (13);
  Calculate $\mathbf{M}_b[k]$ according to Eq. (14);
  Update $\mathbf{A}_b[k] = (\mathbf{M}_b[k])^{-1}$;
  while $\lambda_{max} - \lambda_{min} > \epsilon_1$ **do**
    setting $\lambda_m = \frac{\lambda_{max}+\lambda_{min}}{2}$;
    calculate $\mathbf{F}_{a,fd}[k]$ according to Eq. (21);
    if $\mathrm{tr}\left(\mathbf{F}_{a,fd}[k]\mathbf{F}_{a,fd}^H[k]\right) < 1$ **then**
      $\lambda_{min} = \lambda_m$;
    else
      $\lambda_{max} = \lambda_m$;
    end if
  end while
until The change of $\mathrm{tr}\left(\mathbf{A}_b[k]\mathbf{M}_b[k]\right)$ is below ϵ_2.

First, we calculate $\mathbf{W}_{b,fd}[k]$ according to Eq. (13) and $\mathbf{M}_b[k]$ according to Eq. (14) with fixed $\mathbf{F}_{a,fd}[k]$. Then, we set $\mathbf{A}_b[k] = (\mathbf{M}_b[k])^{-1}$, and update $\mathbf{F}_{a,fd}[k]$. The corresponding Lagrange function to solve $\mathbf{F}_{a,fd}[k]$ can be formulated as follows

$$L_{\mathbf{F}_{a,fd}[k]} = \&\frac{1}{K}\sum_{k=1}^{K}\mathrm{tr}\left(\mathbf{A}_b[k]\mathbf{M}_b[k]\right) + \lambda\left[\mathrm{tr}\left(\mathbf{F}_{a,fd}[k]\mathbf{F}_{a,fd}^H[k]\right) - 1\right], \tag{20}$$

where λ is the Lagrange multiplier. By setting the derivative of $L_{\mathbf{F}_{a,fd}[k]}$ w.r.t. $\mathbf{F}_{a,fd}[k]$ to zero, $\mathbf{F}_{a,fd}[k]$ can be solved as

$$\begin{aligned}\mathbf{F}_{a,fd}[k] = &\big[P_a\bar{\mathbf{H}}_{ab}^H[k]\mathbf{W}_{b,fd}[k]\mathbf{A}_b[k]\mathbf{W}_{b,fd}^H[k]\bar{\mathbf{H}}_{ab}[k] \\ &+ P_a\sigma_{ab}^2\mathrm{tr}\left(\mathbf{A}_b[k]\mathbf{W}_{b,fd}^H[k]\mathbf{R}_b\mathbf{R}_b^H\mathbf{W}_{b,fd}[k]\right)\mathbf{T}_a^H\mathbf{T}_a \\ &+ \lambda\mathbf{I}\big]^{-1}\sqrt{P_a}\bar{\mathbf{H}}_{ab}^H[k]\mathbf{W}_{b,fd}[k]\mathbf{A}_b[k].\end{aligned} \tag{21}$$

Based on Eq. (21), a bisection search method can be adopted to obtain λ. Notice that $\lambda \geq 0$, so we set the minimum Lagrange multiplier as $\lambda_{min} = 0$, and calculate $\mathbf{F}_{a,fd}[k]$. If the power constraint is satisfied, we set $\lambda = 0$. Otherwise, we set the maximum Lagrange multiplier λ_{max} to a pre-defined value and start the bisection search until the power constraint is satisfied. The proposed iterative algorithm is summarized in Algorithm 1.

Due to the alternating minimization process, the objective function in (19) decreases monotonically. Combined with the fact that the WMMSE is lower bounded, the convergence of Algorithm 1 can be guaranteed. A similar approach can be found in [17]. The fully digital beamformers $\mathbf{F}_{b,fd}[k]$ and $\mathbf{W}_{a,fd}[k]$ can be obtained by directly substituting the corresponding matrices into Algorithm 1. We omit further details here to avoid repetitions.

3.3 Hybrid Beamforming Design for Partially-Connected Structure

Different from fully-connected structure, the output signal of each RF chain in the partially-connected structure is connected to a sub-array to improve the energy efficiency and further reduce the hardware implementation complexity. Therefore, the analog beamforming matrix in the partially-connected structure can be formulated as a block diagonal format, and each block is an vector that satisfies the constant modulus constraint. Taking the precoder at node a as an example, each RF chain is connected to $\frac{N_a}{N_{a,rf}}$ antennas, and the analog precoder is given by

$$\mathbf{F}_{a,t} = \text{blkdiag}\left[\mathbf{f}_1, \mathbf{f}_2, \ldots, \mathbf{f}_{N_{rf}}\right] \tag{22}$$

where $\mathbf{f}_i = \left[\exp\left(j\theta_{\frac{(m-1)N_a}{N_{a,rf}}+1}\right), \ldots, \exp\left(j\theta_{\frac{mN_a}{N_{a,rf}}}\right)\right]^T$, $m = 1, \ldots, N_{a,rf}$, with θ_i being the phases of the corresponding phase shifter. So the total number of phase shifters in this structure is N_a, indicating that the hardware complexity of RF beamformers is one $N_{a,rf}$ fold lower than that of fully connected structures.

In this section, we aim for decomposing the fully digital beamformers into hybrid ones with partially connected structure. The hybrid beamformer optimization problem is constructed as an Euclidean distance minimization problem of all the subcarriers, which can be formulated as follows

$$\begin{aligned} \min_{\{\mathbf{F}_{a,t}, \mathbf{F}_{a,bb}[k]\}} & \sum_{k=1}^{K} \|\mathbf{F}_{a,fd}[k] - \mathbf{F}_{a,t}\mathbf{F}_{a,bb}[k]\|^2 \\ \text{s.t.} \quad & \|\mathbf{F}_{a,t}\mathbf{F}_{a,bb}[k]\|_F^2 = 1, \\ & \mathbf{F}_{a,t} \in \mathcal{F} \end{aligned} \tag{23}$$

where $\mathcal{F}$ is the set of feasible analog beamformers induced by the equal-modulus constraint. In our previous work [18], we have proved that if the unconstrained solution for the problem (23) is sufficiently close to $\mathbf{F}_{a,fd}[k]$, the corresponding normalization that satisfies the power constraint can achieve the Euclidean distance in the same order. This conclusion can also be extended to broadband systems. The corresponding unconstrained optimization problem is formulated as

$$\begin{aligned} \min_{\{\mathbf{F}_{a,t}, \mathbf{F}_{a,bb}[k]\}} & \sum_{k=1}^{K} \|\mathbf{F}_{a,fd}[k] - \mathbf{F}_{a,t}\mathbf{F}_{a,bb}[k]\|^2 \\ \text{s.t.} \quad & \mathbf{F}_{a,t} \in \mathcal{F} \end{aligned} \tag{24}$$

We alternatively optimize $\mathbf{F}_{a,t}$ and $\mathbf{F}_{a,bb}[k]$ in the next. In nth iteration, by taking advantage of the special properties of block diagonal structure of $\mathbf{F}_{a,t}$ and with fixed $\mathbf{F}_{a,bb}[k]$, problem (24) can be rewritten as

$$\min_{\theta_i} \& \sum_{k=1}^{K} \| \left(\mathbf{F}_{a,fd}[k]\right)_{i,:} - \exp\left(j\theta_i^{(n)}\right) \left(\mathbf{F}_{a,bb}^{(n)}[k]\right)_{l,:} \|^2 \tag{25}$$

where $l = \lceil i\frac{N_{a,rf}}{N_a} \rceil$. This is a vector rotation problem, and the closed-form solution is given by

$$\&\theta_i^{(n)} = \arg\left\{\sum_{k=0}^{K-1} \left(\mathbf{F}_{a,fd}[k]\right)_{i,:} \left(\mathbf{F}_{a,bb}^{(n)}[k]\right)_{l,:}^{H}\right\}, i = 1, \ldots, N_a. \tag{26}$$

Then, we optimize $\mathbf{F}_{a,bb}[k]$ with the fixed $\mathbf{F}_{a,t}$. Since the digital precoder is optimized for each subcarrier, we can get rid of the summation notation in (24) when optimizing the baseband precoder $\mathbf{F}_{a,bb}[k]$. The closed-form solution is given by

$$\&\mathbf{F}_{a,bb}^{(n)}[k] = \left[\left(\mathbf{F}_{a,t}^{(n)}\right)^H \mathbf{F}_{a,t}^{(n)}\right]^{-1} \left(\mathbf{F}_{a,t}^{(n)}\right)^H \mathbf{F}_{a,fd}[k] \tag{27}$$

The iteration terminates when the change of the objective function is below a pre-defined threshold. At last, $\mathbf{F}_{a,bb}[k]$ is normalized to satisfy the power constraint, which is given by

$$\mathbf{F}_{a,bb}[k] = \frac{\mathbf{F}_{a,bb}[k]}{\|\mathbf{F}_{a,t}\mathbf{F}_{a,bb}[k]\|_F} \tag{28}$$

4 Simulation Results

In the following, we present numerical results of the proposed robust hybrid FD OFDM beamforming designs. The propagation paths for different channels are all set as $Np = 4$. The elements of mmWave channels, i.e., complex gains of propagation paths, and AWGN matrices obey complex Gaussian distribution. Furthermore, the azimuth AoAs and AoDs for each of the channel paths follow Laplacian distribution with uniformly distributed means over $[0, 2\pi)$, and angular spread of 5°. The Rician factor κ in Eq. (6) is set to 20 dB and path gain α is complex Gaussian distributed with zero mean and unit variance. The transmitted powers and SI powers of different links are set to be equal, i.e., $P_a = P_b$, $P_{a,si} = P_{b,si}$. The transmitted signal-to-noise ratio (SNR) is defined as $\text{SNR} = 10\log_{10}\frac{P_i}{\delta_i^2}$, the interference-to-noise ratio (INR) is defined as $\text{INR} = 10\log_{10}\frac{P_{i,si}}{\delta_i^2}$. The termination criteria in Algorithm 1 are set as $\epsilon_1 = \epsilon_2 = 1 \times 10^{-4}$. The maximum number of iterations is set to 50 to control the convergence rate. All the simulations are averaged over 1000 channel realizations.

Figure 1 shows the spectral efficiency comparison between the proposed design for different INR settings with other existing designs. The fully-connected structure design is obtained by replacing sub-connected structures in the proposed design with fully-connected structures. The antenna configurations are set as $N_a = M_a = 64$, $N_b = M_b = 32$, $N_{a,rf} = N_{b,rf} = M_{a,rf} = M_{b,rf} = 4$, $N_{a,s} = N_{b,s} = 2$. The estimation error covariances are $\sigma_{e,aa}^2 = \sigma_{e,bb}^2 = 0.7$. As we can see, the proposed design is only inferior to the fully-connected design. The proposed design outperforms the design in [14] by 11.1% at SNR = 10 dB.

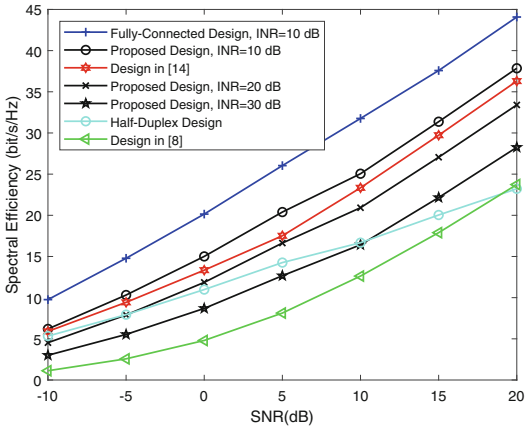

Fig. 1. Spectral efficiency at different SNR settings. $N_a = M_a = 64$, $N_b = M_b = 32$, $N_{a,rf} = N_{b,rf} = M_{a,rf} = M_{b,rf} = 4$, $N_{a,s} = N_{b,s} = 2$, $\sigma^2_{e,aa} = \sigma^2_{e,bb} = 0.7$.

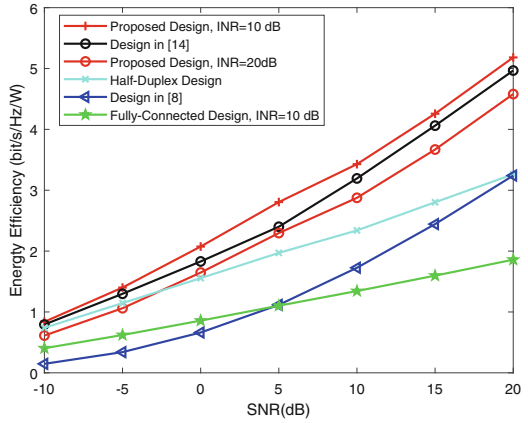

Fig. 2. Energy efficiency at different SNR settings. $N_a = M_a = 64$, $N_b = M_b = 32$, $N_{a,rf} = N_{b,rf} = M_{a,rf} = M_{b,rf} = 4$, $N_{a,s} = N_{b,s} = 2$, $\sigma^2_{e,aa} = \sigma^2_{e,bb} = 0.7$.

When INR goes higher, the performance curves of the proposed designs intersect with the HD mode due to the imperfect SIC effect caused by estimation errors, e.g., the HD mode outperforms the proposed designs when SNR ≤ -5 dB at INR $= 20$ dB and SNR ≤ 10 dB at INR $= 30$ dB. However, the proposed design still prevails the HD mode at high SNR regime, e.g., 20.81% gains can be seen at SNR $= 20$ dB when INR $= 30$ dB. Moreover, when the INR rises to 30 dB, the proposed design still outperforms the design in [8]. The design in [8] suppresses the power of SI plus noise covariance. However, the performance degrades severely under imperfect channel estimations.

Figure 2 plots the energy efficiency comparison of different designs appeared in Fig. 1. The configurations are the same as that in Fig. 1. The power consumption at the base station side for fully-connected structure and partially-structure can be expressed as

$$\begin{aligned} P_{fully} &= N_i(N_{i,rf}+1)P_{LNA} + N_i N_{i,rf} P_{PS} \\ &\quad + N_{i,rf}(P_{RFC}+P_{ADC}) + P_{BB} + N_{i,rf}P_{SI}, \\ P_{sub} &= N_i P_{LNA} + N_i P_{PS} + N_{i,rf}(P_{RFC}+P_{ADC}) \\ &\quad + P_{BB} + N_{i,rf}P_{SI}, \end{aligned}$$

where P_{LAN} denotes the power of the low-noise amplifier; P_{PA} denotes the power of phase shifters. P_{BB} denotes the power of baseband processing; P_{RFC} denotes the power of RF chains; P_{DAC} denotes the power of digital-to-analog converts. The power consumption at the destination can be obtained by corresponding substitutions. The value of each component follows the setting in [6]. As shown in this figure, although the fully-connected design provides higher spectral efficiency, its energy efficiency is the worst. The proposed partially-connected designs provide higher energy efficiency due to the reduced number of phase shifters. The proposed design outperforms the fully-connected design by 174.7% at SNR = 20 dB. Even if the INR is increased to 20 dB, the proposed design still outperforms the design in [8] by 44.6% at SNR = 20 dB and performs closely to the design in [14]. Due to the lower hardware complexity of the HD mode, it provides higher energy efficiency when the SNR is low. With the increase of SNR, its performance is inferior to the proposed design.

5 Conclusions

In this paper, partially-connected structures and correlated estimation errors are considered to develop a robust hybrid beamforming design for FD OFDM mmWave systems. The SI is attenuated by the zero-space projection based method. Then, the fully digital beamformers and the corresponding hybrid ones are solved sequentially. Simulation results verify the superiority of the proposed robust design over other existing designs.

References

1. Heath, R.W., Jr., Gonzalez-Prelcic, N., Rangan, S., Roh, W., Sayeed, A.M.: An overview of signal processing techniques for millimeter wave MIMO systems. IEEE J. Sel. Topics Signal Process. **10**, 436–453 (2016)
2. Xia, X., Xu, K., Wang, Y., Xu, Y.: A 5G-enabling technology: benefits, feasibility, and limitations of in-band full-duplex mMIMO. IEEE Veh. Technol. Mag. **13**(3), 81–90 (2018)
3. Xia, X., Xu, K., Wang, Y., Xu, Y.: Beam-domain full-duplex massive MIMO: realizing co-time co-frequency uplink and downlink transmission in the cellular system. IEEE Trans. Veh. Technol. **66**(10), 8845–8862 (2017)

4. Xu, K., Shen, Z., Wang, Y., Xia, X., Zhang, D.: Hybrid time-switching and power splitting SWIPT for full-duplex massive MIMO systems: a beam-domain approach. IEEE Trans. Veh. Technol. **67**(8), 7257–7274 (2018)
5. Xiao, Z., Xia, P., Xia, X.-G.: Full-duplex millimeter-wave communication. IEEE Wirel. Commun. **24**(6), 136–143 (2017)
6. Zhang, Y., Xiao, M., Han, S., Skoglund, M., Meng, W.: On precoding and energy efficiency of full-duplex millimeter-wave relays. IEEE Trans. Wirel. Commun. **18**(3), 1943–1956 (2019)
7. Satyanarayana, K., El-Hajjar, M., Kuo, P.-H., Mourad, A., Hanzo, L.: Hybrid beamforming design for full-duplex millimeter wave communication. IEEE Trans. Veh. Technol. **68**(2), 1394–1404 (2019)
8. Satyanarayana, K., El-Hajjar, M., Mourad, A., Hanzo, L.: Multi-user full duplex transceiver design for mmWave systems using learning-aided channel prediction. IEEE Access **7**, 66068–66083 (2020)
9. Garcia-Rodriguez, A., Venkateswaran, V., Rulikowski, P., Masouros, C.: Hybrid analog-digital precoding revisited under realistic RF modeling. IEEE Wirel. Commun. Lett. **5**(5), 528–531 (2016)
10. El Ayach, O., Heath, R.W., Rajagopal, S., Pi, Z.: Multimode precoding in millimeter wave MIMO transmitters with multiple antenna sub-arrays. In: 2013 IEEE Global Communications Conference (GLOBECOM), pp. 3476–3480 (2013)
11. Cai, Y., Xu, Y., Shi, Q., Champagne, B., Hanzo, L.: Robust joint hybrid transceiver design for millimeter wave full-duplex MIMO relay systems. IEEE Trans. Wirel. Commun. **18**, 1199–1215 (2019)
12. Jiang, L., Jafarkhani, H.: mmWave amplify-and-forward MIMO relay networks with hybrid precoding/combining design. IEEE Trans. Wirel. Commun. **19**(2), 1333–1346 (2020)
13. Park, S., Alkhateeb, A., Heath, R.W.: Dynamic subarrays for hybrid precoding in wideband mmWave MIMO systems. IEEE Trans. Wirel. Commun. **16**(5), 2907–2920 (2017)
14. Yu, X., Shen, J.-C., Zhang, J., Letaief, K.B.: Alternating minimization algorithms for hybrid precoding in millimeter wave MIMO systems. IEEE J. Sel. Topics Signal Process. **10**(3), 485–500 (2016)
15. Luo, Z., Zhao, L., Tonghui, L., Liu, H., Zhang, R.: Robust hybrid precoding/combining designs for full-duplex millimeter wave relay systems. IEEE Trans. Veh. Technol. **70**(9), 9577–9582 (2021)
16. Xing, C., Ma, S., Fei, Z., Wu, Y.-C., Poor, H.V.: A general robust linear transceiver design for multi-hop amplify-and-forward MIMO relaying systems. IEEE Trans. Signal Process. **61**(5), 1196–1209 (2013)
17. Christensen, S.S., Agarwal, R., de Carvalho, E., Cioffi, J.M.: Weighted sum-rate maximization using weighted MMSE for MIMO-BC beamforming design. IEEE Trans. Wirel. Commun. **7**(12), 4792–4799 (2008)
18. Luo, Z., Zhao, L., Liu, H., Li, Y.: Robust hybrid beamforming in millimeter wave systems with closed-form least-square solutions. IEEE Wirel. Commun. Lett. **10**(1), 156–160 (2021)